Chinese Chemical Letters 37 (2026) 112072

Contents lists available at ScienceDirect

Chinese Chemical Letters

journal homepage: www.elsevier.com/locate/cclet

Stratum corneum-inspired all-natural-based biogel dressing for promoting infected wound healing

Zhi-Guo Wang[a,1], Wen-Ling Du[b,1], Jing Sun[c], Jun-Jie Xiao[b], Yuan-Yuan Mou[d], Xue Xiao[e], Lingli Li[d], Lin Zeng[f], Bai-Song Zhao[g,*], Jia-Zhuang Xu[b], Min Yang[h,*], Zhong-Ming Li[b,i]

[a] *Medicine and Engineering Interdisciplinary Research Laboratory of Nursing & Materials, West China Hospital, Sichuan University/West China School of Nursing, Sichuan University, Chengdu 610041, China*
[b] *College of Polymer Science and Engineering, State Key Laboratory of Advanced Polymer Materials, Sichuan University, Chengdu 610065, China*
[c] *Department of Anesthesiology, Shenzhen Futian District Maternity & Child Healthcare Hospital, Shenzhen 518000, China*
[d] *West China Hospital, Sichuan University/West China School of Nursing, Sichuan University, Chengdu 610041, China*
[e] *Laboratory of Gastric Cancer, State Key Laboratory of Biotherapy, Collaborative Innovation Center of Biotherapy and Cancer Center, West China Hospital, Sichuan University, Chengdu 610065, China*
[f] *President & Dean's Office, West China Hospital, Sichuan University, Chengdu 610041, China*
[g] *Department of Anesthesiology, Zhujiang Hospital, Southern Medical University, Guangzhou 510000, China*
[h] *Division of Oncology, Department of Paediatric Surgery, West China Hospital, Sichuan University, Chengdu 610041, China*
[i] *Institute of Cardiovascular Surgery, West China Hospital, Sichuan University, Chengdu 610041, China*

ARTICLE INFO

Article history:
Received 11 August 2025
Revised 5 November 2025
Accepted 6 November 2025
Available online 7 November 2025

Keywords:
Infected wound
Hydrogel dressing
Natural moisturizing factor
Mechanical strength
Antibacterial property

ABSTRACT

Natural material-based hydrogels have emerged as ideal candidates for serving as infected wound dressings relying on the extracellular matrix-like microstructure, biocompatibility and the supplying of the wet healing microenvironment. Nevertheless, these hydrogels suffer from limitations including the weak mechanical property, poor water retention ability and inadequate antibacterial property. Herein, we develop a stratum corneum-inspired all-natural-based biogel dressing by directly incorporating natural moisturizing factor (NMF) into gelatin/chitosan quaternary ammonium salt (QCS) hydrogels without necessitating any chemical modification. The sodium pyrrolidone carboxylic acid (PCA-Na, an NMF compound) equipping carboxyl groups forms the ionic crosslink with gelatin containing protonated amino groups and QCS involving quaternary ammonium groups by electrostatic interaction, leading to a significant melioration in the mechanical strength of the biogel. The highly hydrophilic PCA-Na contributes to form additional hydrogen bonds and heighten resistance to dehydration of the biogel, mimicking the role of NMF in the stratum corneum. The excellent broad-spectrum antibacterial property, temperature-controlled reversible fluid-gel transition property and complete degradability are also gathered. A *Staphylococcus aureus*-infected full-thickness wound repair experiment manifests that our biogel effectively promotes infected wound healing by inhibiting inflammatory factors, facilitating formation of the granulation tissue and angiogenesis. This work paves a valuable way for designing multifunctional natural material-based hydrogel dressings.

© 2026 Published by Elsevier B.V. on behalf of Chinese Chemical Society and Institute of Materia Medica, Chinese Academy of Medical Sciences.

The skin is the most susceptible organ of the human body for the appearance of wounds that generate an open portal between interior tissues/organs and the external environment [1–3]. Exposed skin wounds provide a warm and humid microenvironment for bacterial colonization and proliferation, resulting in the occurrence of bacterial infection that severely impedes the healing trajectory [4–6]. Infected wounds are trapped in the inflammatory phase for a long time, hampering the proliferative and remodeling phases of wound healing and causing delayed or even incapable wound healing [7,8]. Clinical treatments of infected wounds commonly employ wound dressings including cotton, gauze and bandages to provide a dry healing environment, but the repair of infected wounds is seriously restricted owing to the absence of the antibacterial ability [9,10]. Antibiotic administration is an effective clinical therapy for healing infected wounds, but carries a high risk of antibiotic resistance [11,12].

* Corresponding authors.
E-mail addresses: zhaobaisong819@163.com (B.-S. Zhao), hx2014bsym@163.com (M. Yang).
[1] These authors contributed equally to this work.

https://doi.org/10.1016/j.cclet.2025.112072
1001-8417/© 2026 Published by Elsevier B.V. on behalf of Chinese Chemical Society and Institute of Materia Medica, Chinese Academy of Medical Sciences.

Natural material-based hydrogel dressings composed of gelatin, chitosan, alginate, *etc.* emerge as highly competitive candidates for promoting infected wound healing, due to the extracellular matrix (ECM)-like microstructure, biocompatibility, an optimal wet healing microenvironment and biodegradation [13–15]. The improvement of the antibacterial property of natural-based hydrogel dressings was already achieved by introducing quaternary ammonium, N-hal-amine and phenols, *etc.* [16,17]. Unluckily, poor mechanical properties make natural polymeric hydrogels vulnerable to external forces or the body movement, causing the structural damage and compromission of the therapeutic efficiency [18,19]. Besides, a poor water retention capacity of natural-based hydrogels generally results in the reduction of flexibility and functionality, shortening the service time as wound dressings [20–22]. A myriad of efforts have been devoted to addressing these challenges, including introducing chemically crosslinked networks or nano-fibers/fillers to enhance mechanical properties, and incorporating glycerol or high-density hygroscopic salts to meliorate the water retention ability [23]. Nevertheless, these strategies suffer from the production of a toxic effect, complex preparation process, and the difficulty in concurrent improvement of mechanical and water retention properties.

The stratum corneum, the outermost layer of the skin, contains the natural moisturizing factor (NMF) to maintain moisture in the skin [24]. NMF encapsulated in the corneocytes is a mixture of water-soluble compounds. And it is indispensable for ameliorating the mechanical extensibility of the stratum corneum and preventing excessive water loss from the skin [25]. In this work, we engineered a stratum corneum-inspired all-natural-based biogel dressing integrating high mechanical strength and elongation, excellent water retention capacity and broad-spectrum antibacterial features for treating infected wounds. Sodium pyrrolidone carboxylic acid (PCA-Na) was selected as NMF and formed the ionic crosslink with gelatin and chitosan quaternary ammonium salt (QCS), significantly improving the mechanical strength and elongation of the biogel. The water retention capacity of the biogel was synchronously meliorated surpassing the pure gelatin/QCS hydrogel, ascribed to the formation of abundant hydrogen bonds between PCA-Na and water molecules. The high antibacterial efficiency against *Staphylococcus aureus* (*S. aureus*) and *Escherichia coli* (*E. coli*) accompanied by a favorable biocompatibility and injectability was also substantiated. *In vivo* evaluation based on a rat infected wound model further demonstrated that our biogel effectively promoted wound healing. The current work provides an appealing and effective prototype for fabricating advanced infected wound dressings.

Fig. 1a illustrates the schematic fabrication process for the biogel. Stratum corneum contains NMF with a low vapor pressure that exhibiting a promising potential in replacing water under dry conditions and mitigating dehydration-caused changes in the lipid and protein compositions of the skin. Furthermore, NMF is able to improve extensibility and elasticity of the stratum corneum by engaging the ionic interaction. To modulate properties of the biogel, PCA-Na, a major component of NMF, was selected as the crosslinker to add into the QCS/gelatin solution at a high temperature. The gelatin/QCS/PCA-Na (called as GQSP) solution undergoes the change from fluid to gel to obtain the GQSP biogel by simply cooling to 37 °C (Fig. 1b). It is worth noting that the gel-to-fluid state transition of the GQSP biogel occurs when the temperature returns to 50 °C, indicating the reversible preparation of the biogel [26,27]. It is ascribed to the thermo-reversible phase transition characteristic of gelatin, whose chain structures transform between random coils and triple helices. The temperature-dependent phase transition property endows the GQSP biogel with the capacity for *in situ* gelation. Figs. 1c–e show that the fluidic GQSP biogel covering the seashell and leaf spontaneously converts to a gel state and replicates the surface texture with complex microscopic cur-

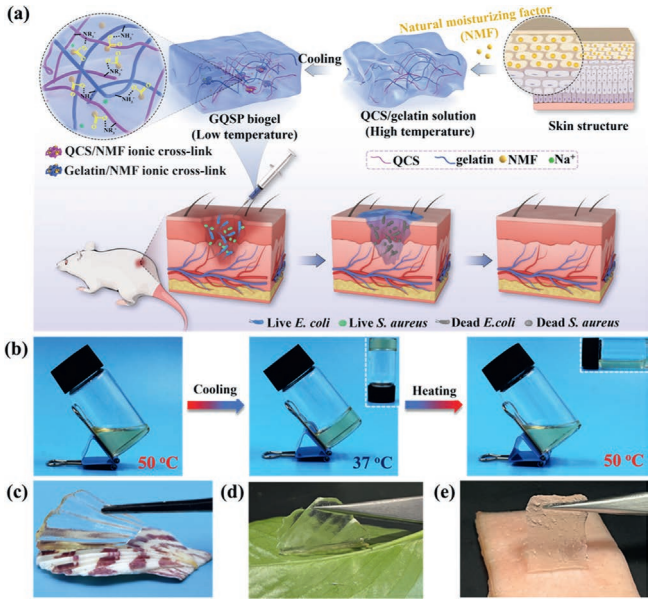


Fig. 1. Construction of the GQSP biogel and conformal contact with surfaces with complex shapes. (a) Schematic illustration of the preparation process of the GQSP biogel. (b) The reversible sol-gel transition of the biogel through altering the temperature. (c–e) Photographs of the biogel after *in situ* gelation.

vatures. The excellent *in situ* gelation property is also manifested by the well-preserved morphology of the pig skin on the surface of the GQSP biogel.

Microstructural observation displays that the average pore size of the GQSP biogel embedded PCA-Na is notably smaller than the pure QCS/gelatin (GQSP0) hydrogel, indicative of enhancement of the cross-link density (Fig. 2a). Compared with the GQSP0 biogel, an evident decrease in the carbon (C) element and a synchronous increase in the oxygen (O) and sodium (Na) elements are perceptible for the GQSP biogel with the additive PCA-Na. This decreasing trend of the C element is more pronounced with the enhancement of the PCA-Na content. Furthermore, the homogeneous distribution of the Na element indicates the uniformity of PCA-Na. XPS analysis was conducted to further investigate components of the GQSP biogel. Additional characteristic peaks of Na appear in the XPS spectrum of the GQSP60 biogel compared to the GQSP0 biogel (Fig. 2b). The C 1s spectrum of the GQSP biogel is deconvoluted into three peaks assigned to the C1 (C–H/C–C), C2 (C–N/C–O/C=N), and C3 (C=O) peaks. The markedly increasing peak area of the C2 peak for the GQSP60 biogel in comparison to the GQSP0 biogel reveals the incorporation of PCA-Na (Figs. 2c and d).

The healing of the GQSP60 biogel is readily achieved through localized melting around a crack using a heat source (Fig. 2e). Upon exposure to the heat source, the biogel edges near the crack are heated and transformed into a fluidic state owing to the temperature-controlled phase transition property of the biogel. The localized liquefaction process efficiently promotes the healing of cracks of the biogel. The special healing mechanism provides an attractive structural foundation for simply and rapidly healing the damaged GQSP biogel serving as a wound dressing by localized heat sources (*e.g.,* infrared light). The GQSP precursor solution is able to be extruded from a syringe with a needle to acquire the biogel fiber and “write” word of SCU under the high temperature. Such exceptional injectability allows the biogel to directly fill desired wounds with diverse shapes and assure a perfect fit with the target region. Intricately shaped biogels including the heart and star are accurately obtained by transferring the GQSP precursor solution into moulds and subsequent cooling (Fig. 2f).

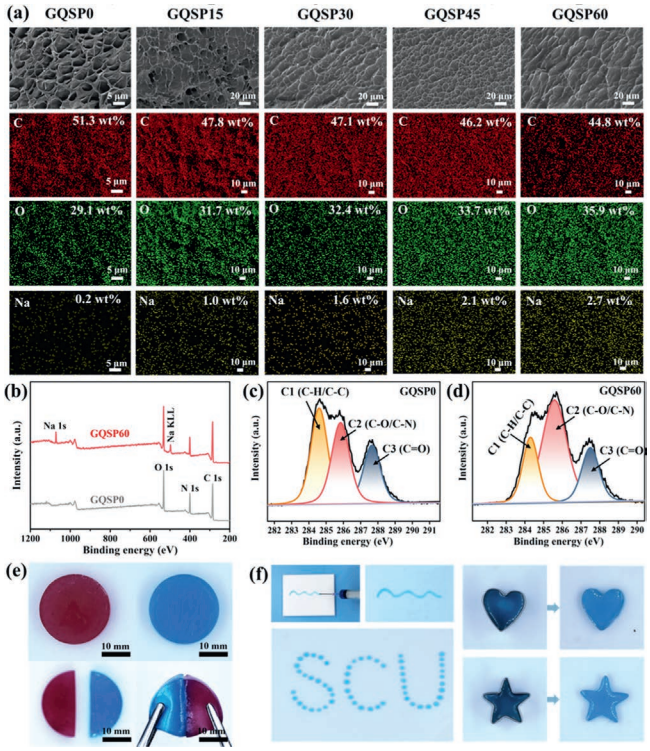


Fig. 2. Microstructure, component analysis, healing and injectability of the GQSP biogel. (a) SEM images and EDS elemental mapping of the biogel. (b) The XPS spectra of the GQSP0 and GQSP60 biogels. The high-resolution C 1s XPS spectra of (c) the GQSP0 and (d) GQSP60 biogels. (e) Photos of healing of the GQSP60 biogel by localized heating. (f) The biogel fiber and word obtained by injecting the GQSP60 solution and photos of the biogel constructs.

The robust mechanical property is momentous for hydrogel dressings to avoid destruction of the structural integrity when exposed to exterior damage. A notable improvement of the mechanical property is visible with the escalating PCA-Na concentration (Fig. 3a). Especially, the tensile strength and elongation at break of the GQSP60 hydrogel are 104.6 kPa and 244.5 %, 280 % and 235 % higher than them of the GQSP0 biogel respectively (Fig. 3b). Similar trend is observed in the elastic modulus of the GQSP60 biogel (Fig. S1 in Supporting information). To disclose the underlying mechanism of the ameliorative mechanical property, the rheological feature of the GQSP biogel with respect to varied temperatures was investigated. After introducing PCA-Na, the complex viscosity of the GQSP60 biogel significantly increases compared with the GQSP0 biogel (Fig. 3c). The apparent incremental tendency is perceived in the storage modulus (G') and loss modulus (G'') of the GQSP60 biogel during the cooling process (Fig. 3d). The relevant tanδ (G''/G') values indicate that the transition temperature from viscous liquid to viscoelastic gel rises from 36.6 °C for the GQSP0 biogel to 39.1 °C for the GQSP60 biogel (Fig. 3e). The changed rheological behavior is attributed that the thermal-responsive phase transition results from the adjustment of physical crosslinks in the GQSP biogel across varied temperature regimes. The augmentation of the fluid-gel transition temperature is bound up with the increasing cross-link density of the GQSP60 biogel. The densely packed hydrogel network with intensified crosslinking density of the GQSP biogel effectively transfers and dissipates the tensile stress to achieve the melioration of mechanical strength and elongation.

The interaction between PCA-Na and the matrix of the GQSP biogel determines the cross-linked hydrogel network. Fig. 3f presents that the Amide I and Amide II bands display a discernible redshift with the incorporation of PCA-Na in the Fourier transform infrared spectroscopy (FTIR) spectra of the GQSP biogel. The characteristic peaks at 1631 cm^{-1} (Amide I) and 1541 cm^{-1} (Amide II) for the GQSP0 biogel shift to 1633 and 1543 cm^{-1} for the GQSP60 biogel, respectively. This redshift demonstrates the formation of strong electrostatic attraction between the negatively charged carboxyl groups in PCA-Na and the positively charged amide groups in gelatin as well as quaternary ammonium groups in QCS. The Amide A band at 3296 cm^{-1} for the GQSP0 biogel shifts to a lower wavenumber of 3284 cm^{-1} for the GQSP60 biogel, indicative of enhanced numbers of hydrogen bonds induced by the introduction of PCA-Na [28]. Further evidence was accessed by Raman spectra. The GQSP60 biogel displays a distinct peak associated with C–O stretching, owing to the addition of carboxyl groups from PCA-Na (Fig. 3g). The Amide I absorption peak presents a slight blueshift, indicating the formation of intermolecular interactions between PCA-Na and the gelatin as well as QCS. The Amide A peak assigned to N–H and O–H stretching of the GQSP60 biogel shifts to higher wavenumbers compared with the GQSP0 biogel, suggesting the increase of hydrogen bonds [29]. Additionally, water confined within the densified hydrogel network of the GQSP60 biogel exhibits a conspicuous reduction of the thawing temperature (−2.7 °C), compared with the GQSP0 biogel with the sparse hydrogel network (1.1 °C) (Fig. 3h), further supporting the aforementioned findings.

The schematic diagram illustrating the intermolecular interactions in the GQSP biogel is shown in Fig. 3i. The amino groups of gelatin and QCS are protonated and yield NH^{3+} entities. These NH^{3+} groups and the quaternary ammonium group of QCS participate in the electrostatic attractions with the carboxyl groups of PCA-Na, forming the ionic crosslink network. The hydrophilic carboxyl groups of PCA-Na contribute to forming abundant hydrogel bonds with free water molecules, inhibiting the dehydration and imparting the GQSP biogel with the excellent water retention ability. The GQSP biogel suffers from dehydration and the weight loss until reaching an equilibrium state, when storing under the ambient conditions (Fig. 3j). The incorporation of PCA-Na prominently reduces the dehydration-related weight loss of the GQSP biogel. For instance, the water retention ratio of the GQSP60 biogel is up to 40 %, 45 % higher than that of the GQSP0 biogel. The excellent water retention ability is conductive to the long-term application of the GQSP biogel as a wound dressing.

To highlight the superiority of the GQSP biogel, different QCS/gelatin hydrogels embedded other additives were prepared and compared (Fig. 3k and Fig. S2 in Supporting information). The incorporation of glycerol, a commonly utilized additive for improving the water retention ratio of hydrogels, into the QCS/gelatin hydrogel ameliorates the water retention ability but diminishes tensile strength [30]. The introduction of sodium citrate, a widely employed additive to enhance the mechanical strength of gelatin hydrogels, into the QCS/gelatin hydrogel leads to the improved tensile strength but compromised water retention capability [31]. In stark contrast, the addition of PCA-Na into the QCS/gelatin hydrogel achieves concurrent melioration in both the water retention capacity and mechanical strength. We propose that introducing NMF compounds with carboxyl groups and free mobile ions is a universal strategy to optimize the mechanical property and water retention capacity of the biogel by amino-anion cross-linking. To demonstrate this hypothesis, sodium lactate was selected as another representative NMF additive for the biogel (named as GQSS) preparation. The resultant GQSS biogel also exhibits the enhanced tensile strength and water retention ability analogous to the GQSP biogel (Figs. S3 and S4 in Supporting information). These findings manifest that NMF compounds including PCA-Na and sodium lactate that possessing carboxyl groups and movable ions are exceptional additives for preparing natural biogel with desired functionalities.

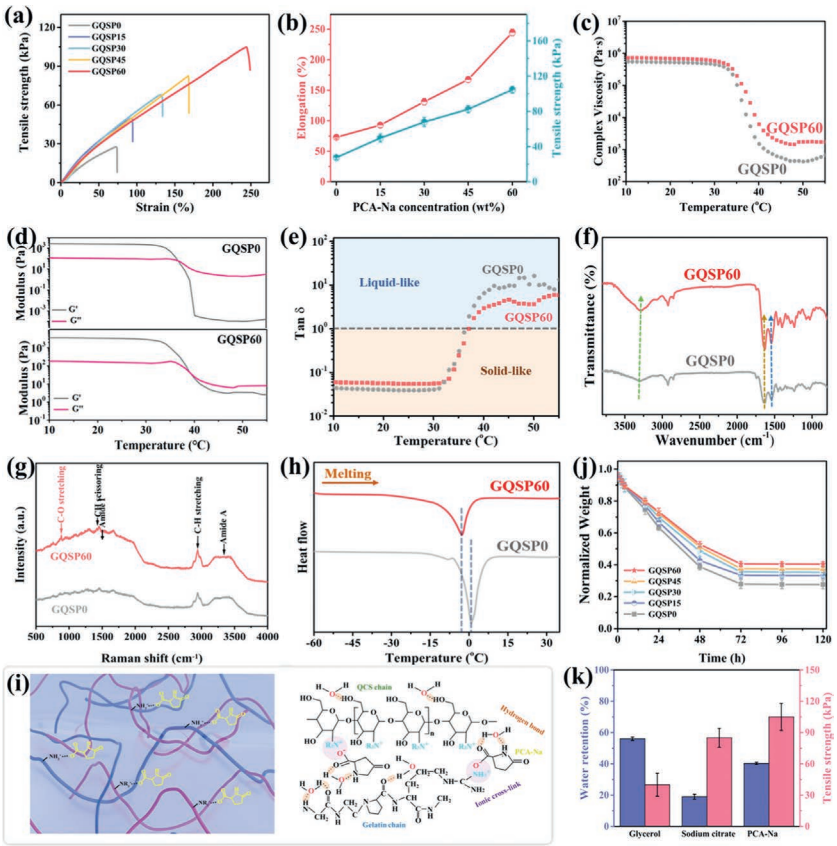


Fig. 3. The mechanical property, water retention capacity, rheology and the component interaction of the GQSP biogel. (a) The stress-strain curves, (b) tensile strength and elongation of the GQSP biogel as a function of the PCA-Na content. The (c) complex viscosity, (d) storage modulus (*G'*) and loss modulus (*G''*) as well as (e) tan*δ* of the GQSP0 and GQSP60 biogels. (f) FTIR spectra, (g) DSC curves and (h) Raman spectra of the GQSP0 and GQSP60 biogels. (i) Schematic diagram of the interaction between PCA-Na and gelation and QCS chains. (j) The dehydration process of the GQSP biogel. (k) Comparison of the water retention ratio and tensile strength of hydrogels with different additives. Data are presented as mean ± standard deviation (SD) ($n = 5$).

Biocompatibility is a crucial precondition for bioactive hydrogels in clinical wound dressing applications [32,33]. The cytocompatibility of the GQSP biogel was assessed using L929 fibroblasts. The live/dead cell staining shows that the majority of L929 cells with a spindle-like morphology are stained in green (live cells) and almost no perceptible cells are stained in red (dead cells), after co-culturing with the biogel extract for 3 days (Fig. 4a). The quantitative cell viability of the GQSP biogel always exceeds 110 % after 1, 2 and 3 days of incubation with L929 cells (Fig. 4b). *In vitro* hemolysis test manifests that the hemolysis rate of the GQSP biogel is around 2 %, meeting the international standard of biomaterials (<5 %) (Fig. 4c). The excellent cytocompatibility and blood compatibility guarantee the biosafety of the GQSP biogel serving as wound dressings. Fibroblast migration is an initial and critical demand for ECM reconstruction during wound healing [34,35]. The cell scratch test indicates that the GQSP biogel effectively promotes L929 cell migration compared with the control group (Fig. 4d). Noteworthily, the GQSP60 biogel exhibits the highest cell migration-promoting ability. After co-culturing with L929 cells for 48 h, the unhealed relative scratch area of the GQSP60 biogel is only 3.5 %, much lower than that of the GQSP0 (10.4 %) and control (100 %) groups (Fig. 4e).

The evaluation of antibacterial property of the GQSP biogel *in vitro* is shown in Figs. 4f and g. *E. coli* and *S. aureus* are selected as the representatives of Gram-negative and Gram- positive bacteria, respectively. The visible colony formation units of *E. coli* and *S. aureus* are substantially reduced after contacting with the GQSP60 biogel for 6 h in contrast to the control group. Detailedly, the GQSP60 biogel displays a superior antibacterial ratio of 99.98 % against *E. coli* and 99.96 % against *S. aureus*, supported by the live/dead staining assay of bacteria. The positively charged quaternary ammonium groups of QCS interact negatively charged bacteria by the electrostatic force leading to cell lysis and death [36–38]. On the other hand, the quaternary ammonium groups of QCS contribute to changing the permeability of the bacterial cell wall and decreasing the normal flow of critical nutrients into the cell to kill bacteria. The degradation experiment shows that the volume of the GQSP60 biogel continuously decreases with the degradation time at 37 °C and it is disintegrated into the constituent building blocks within 5 h (Fig. S5 in Supporting information).

A *S. aureus*-infected full-thickness skin wound model was established in Sprague-Dawley rats to assess the efficacy of the GQSP biogel in promoting infected wound healing (Fig. 5a). All animal experiments were conducted with the approval of the Institutional Animal Care and Use Committee (IACUC) of Sichuan University (approval No. SCU46–2312–02). Model rats were stochastically divided into three groups, receiving treatments with nothing (the control group), the Tegaderm film (the 3M group) and the GQSP60 biogel (the GQSP60 group). After 3 days of treatment, infected wounds still present obvious yellow pus secretion and certain closure for the control and 3M groups. By contrast, the GQSP60-treated wound exhibits apparent contraction and no pus is observed (Fig. 5b). The outstanding antibacterial activity of the GQSP60 biogel facilitates the infection clearance and the transformation from the inflammatory stage to the proliferation stage in wound healing. After treating with the GQSP60 biogel for 7 days, the unhealing wound area ratio is only 3.8 %, much lower than that for the control (34.2 %) and 3M (14.4 %) groups. On day 14, the wound in the GQSP60 group is almost completely healed, different from the visually open

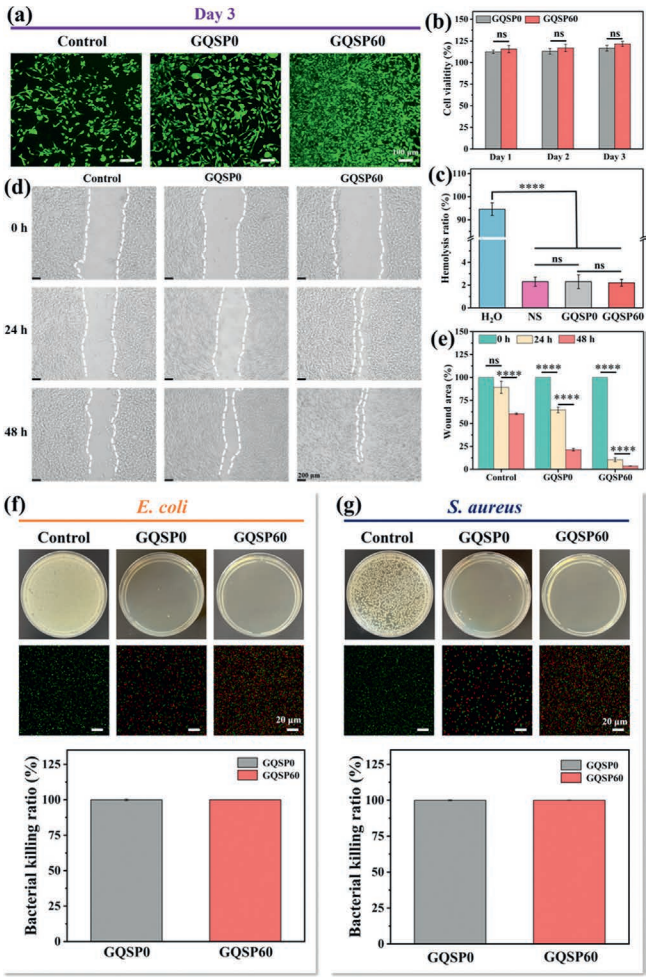


Fig. 4. Biocompatibility, cell migration and antibacterial property of the GQSP biogel *in vitro*. (a) The live/dead staining and (b) cell viability of L929 cells after incubation in the biogel leachate. Scale bar: 100 μm. (c) Hemolysis ratio of the GQSP biogel. The (d) images and (e) quantitative wound area of cell migration after being treated with the GQSP biogel. The representative photos, live/dead staining images and antibacterial ratio of (f) *E. coli* and (g) *S. aureus*. Scale bar: 20 μm. Error bar represents ± SD ($n = 5$). $^{****}P < 0.0001$. ns, no significance.

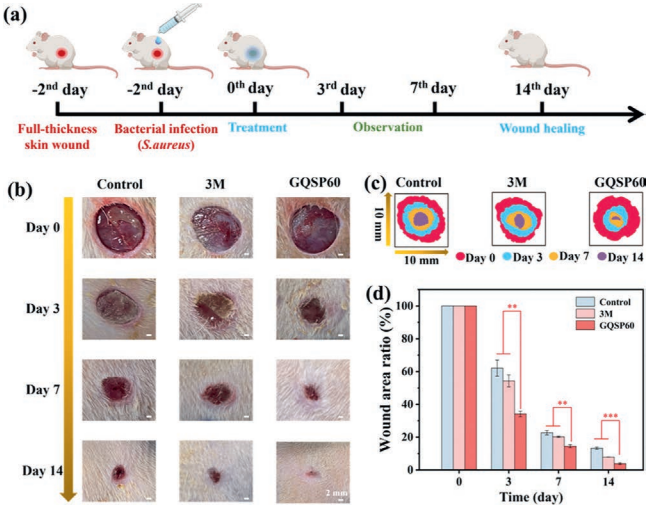


Fig. 5. *In vivo* evaluation of the GQSP60 biogel for *S. aureus*-infected wound healing. (a) Schematic diagram of the experimental procedure. (b) Representative photographs of the wound area after different treat time. (c) Diagram of the wound healing process. (d) Wound area ratios at different time in each group. Error bar represents ± SD ($n = 3$). $^{**}P < 0.01$, $^{***}P < 0.001$.

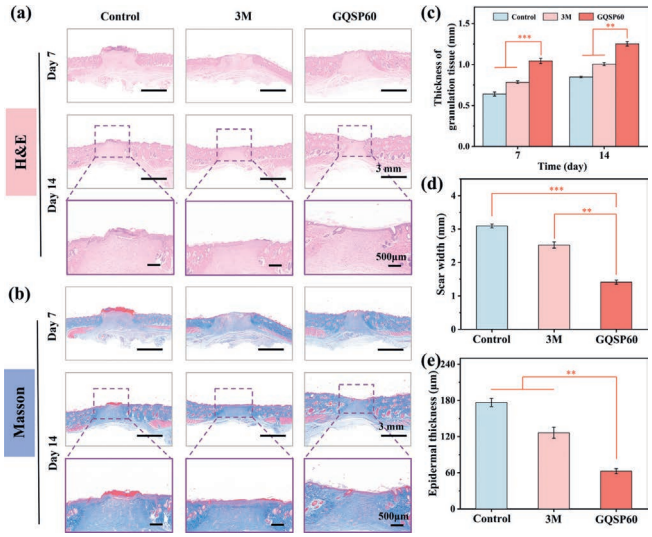


Fig. 6. Histological evaluation of skin wounds after the GQSP60 biogel treatment. (a) H&E staining and (b) Masson trichrome staining of wound tissues on day 7, 14. (c) The thickness of the granulation tissue on day 7, 14. The quantitative analysis of (d) the wound scar width and (e) the epidermal thickness on day 14. Error bar represents ± SD ($n = 3$). $^{**}P < 0.01$, $^{***}P < 0.001$.

wounds for the control and 3M groups, supported by the diagram of varied wound tracings (Fig. 5c). The GQSP60 group possesses the minimum residual wound area ratio of 0.5 %, compared with the control and 3M groups (Fig. 5d). These results highlight that the GQSP60 biogel significantly accelerates infectious wound healing.

Histopathological analysis was performed on wound tissue sections by hematoxylin and eosin (H&E) and Masson staining to assess tissue regeneration on the infected wound bed (Figs. 6a and b). Apparently, the GQSP60 biogel significantly promotes the formation of the granulation tissue with the thickness of 1.25 mm after 14 days of treatment. The control and 3M groups have a deficient promoting effect for generating granulation tissues and the corresponding thickness is only 0.85 and 1.00 mm on day 14 (Fig. 6c). The width of the wound scar reflects the reconstruction efficiency of damaged tissues. The GQSP60 group exhibits the lowest scar width of 1.41 mm, compared with the control (3.09 mm) and 3M (2.52 mm) groups on day 14 (Fig. 6d). Masson staining confirms that the high epidermal integrity and continuity is perceived in the GQSP60 group. The quantitative epidermal thickness for the GQSP60-treated wound is 62.6 μm, 65 % and 50 % lower than that for the control and 3M groups (Fig. 6e). Besides, almost intact re-epithelialization and different skin appendages (like hair follicles) are visible in the GQSP60 group. These findings confirm the excellent therapeutic efficacy of the GQSP60 biogel for infected wounds.

The imbalance of inflammatory cytokines is the important factor for impeding infected wound healing. Interleukin-6 (IL-6) is a typical pro-inflammatory cytokine and one of the most critical markers reflecting the degree of inflammation at the wound site [39]. Immunofluorescence staining shows that the relative expression of IL-6 for the GQSP60 group (38.9 %) is substantially decreased compared to the control (100 %) and 3M (81.1 %) groups (Figs. 7a and b). The remarkable bactericidal activity of the GQSP60 biogel efficiently removes bacterial infection and suppresses inflammation. Neovascularization provides oxygen and nutrients to the cells in the skin tissue and plays a critical role in wound repair [40]. Cluster differentiation 31 (CD31) and vascular endothelial growth factor (VEGF) are typical angiogenesis markers to assess regeneration of new blood vessels [41]. The relative expression of CD31 is prominently higher in wound tissue sections in the GQSP60 group (178 %) than in the control (100 %) and 3M (114 %)

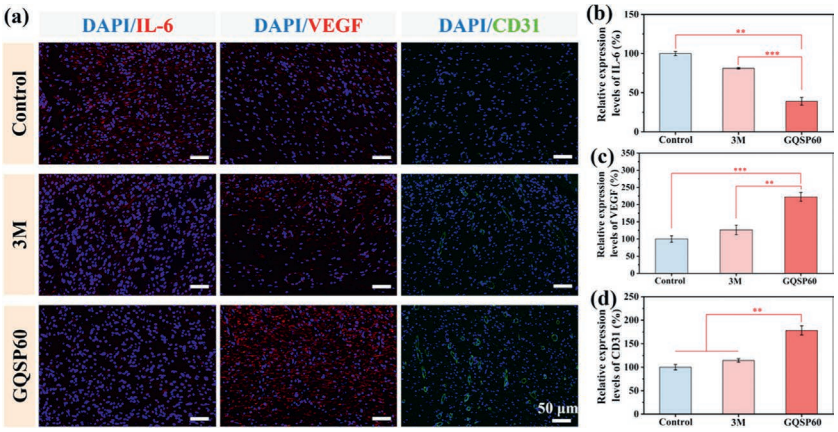


Fig. 7. Immunofluorescence analysis of the wound tissues after different treatments. (a) Photos with immunofluorescence staining of IL-6 (red), CD31 (green), and VEGF (red) in each group on day 14. The relative expression of (b) IL-6, (c) CD31 and (d) VEGF analyzed using ImageJ, respectively. Error bar represents ± SD ($n = 3$). $^{**}P < 0.01$, $^{***}P < 0.001$. DAPI, 4′,6-diamidino-2-phenylindole.

groups on day 14 (Fig. 7c). Similarly, the GQSP60 biogel effectively promotes the relative expression of VEGF (222 %), much higher than the control (100 %) and 3M (126 %) groups (Fig. 7d). Taken together, the GQSP60 biogel significantly reduces the inflammatory response and promote angiogenesis to accelerate wound closure.

In summary, we fabricated a stratum corneum-inspired all-natural-based biogel dressing for infected wound healing. PCA-Na was introduced and formed ionic crosslink with gelatin and QCS by virtue of electrostatic interaction. Furthermore, hydrophilic carboxyl groups of PCA-Na contributed to form additional hydrogen bonds with water molecules. The resultant biogel exhibited improved mechanical strength and elongation and water retention ability compared to the pure gelatin/QCS hydrogel. The remarkable antibacterial property against *E. coli* and *S. aureus*, temperature-controlled reversible phase transition property and degradability were also demonstrated. *In vivo* rat model indicated that the biogel significantly accelerated infected wound healing by reducing inflammation, expediting the formation of granulation tissue and vascularization. Our work offers a paradigmatic means to prepare high-performance natural material-based hydrogel dressings for infected wound healing.

CRediT authorship contribution statement

Zhi-Guo Wang: Writing – review & editing, Funding acquisition, Conceptualization. **Wen-Ling Du:** Writing – original draft, Methodology, Investigation. **Jing Sun:** Validation, Methodology. **Jun-Jie Xiao:** Validation, Formal analysis. **Yuan-Yuan Mou:** Visualization, Investigation. **Xue Xiao:** Visualization, Validation. **Lingli Li:** Validation, Methodology. **Lin Zeng:** Visualization. **Bai-Song Zhao:** Writing – review & editing, Methodology, Funding acquisition. **Jia-Zhuang Xu:** Writing – review & editing, Validation. **Min Yang:** Writing – review & editing, Conceptualization. **Zhong-Ming Li:** Writing – review & editing, Supervision.

Declaration of competing interest

The authors declare that they have no known competing financial interests or personal relationships that could have appeared to influence the work reported in this paper.

Acknowledgments

The authors gratefully thank the financial support from the National Natural Science Foundation of China (Nos. 52403042, 52033005, 82171219), State Key Laboratory of Advanced Polymer Materials (No. sklpme2023–2–13), and National Natural Science Foundation of Guangdong (No. 2024A1515012881).

Supplementary materials

Supplementary material associated with this article can be found, in the online version, at doi:10.1016/j.cclet.2025.112072.

References

[1] P. Wang, H. Li, X. Zhang, et al., Nat. Commun. 16 (2025) 3085.
[2] H. Chen, R. Zhang, G. Zhang, et al., Adv. Mater. 37 (2025) e2410845.
[3] E. Footner, K. Firipis, E. Liu, et al., ACS Biomater. Sci. Eng. 9 (2023) 5933–5952.
[4] W. Liu, C. Yang, R. Gao, et al., Adv. Healthc. Mater. 10 (2021) e2101247.
[5] Y. Gao, L. Wang, C. Zhou, et al., Chin. Chem. Lett. 36 (2025) 110028.
[6] J. Du, C. Xian, X. Liang, et al., Med. Comm. Biomater. Appl. 4 (2025) e70019.
[7] Z. Tu, Y. Zhong, H. Hu, et al., Nat. Rev. Mater. 7 (2022) 557–574.
[8] X. Zhang, R. Li, S. Li, et al., Int. J. Biol. Macromol. 308 (2025) 142280.
[9] C. Yang, G. Liu, J. Chen, et al., Carbohydr. Polym. 282 (2022) 119130.
[10] Z. Li, J. Chen, W. Cao, et al., Carbohydr. Polym. 180 (2018) 192–199.
[11] P.P. Kalelkar, M. Riddick, A.J. Garcia, Nat. Rev. Mater. 7 (2022) 39–54.
[12] M. Wang, T. Li, J. Tian, et al., ACS Nano 18 (2024) 395–409.
[13] X. Zhang, M. Qin, J. Jia, et al., Int J Biol. Macromol. 290 (2025) 139112.
[14] S. Lu, H. Wu, S. Ge, et al., Adv. Healthc. Mater. 13 (2024) 2304676.
[15] L. Wang, L. Sun, Z. Gu, et al., Bioact. Mater. 15 (2022) 330–342.
[16] Y. Ma, X. Zhou, Z. Mo, et al., Int. J. Biol. Macromol. 268 (2024) 131871.
[17] Y. Zhang, Z. Tang, L. Chen, et al., J. Control. Release 378 (2025) 961–981.
[18] C. Hong, H. Chung, G. Lee, et al., Biomacromolecules 25 (2024) 4344–4357.
[19] H. Baniasadi, Adv. Colloid Interface Sci. 342 (2025) 103527.
[20] K. Xu, X. Sun, C. Chong, et al., ACS Appl. Mater. Interfaces 16 (2024) 2027–2040.
[21] X.Q. Wang, A.Q. Xie, P. Cao, et al., Adv. Mater. 36 (2024) e2309952.
[22] L. Dong, Z. Han, H. Zhang, et al., Int. J. Biol. Macromol. 208 (2022) 530–543.
[23] Y. Li, W. Song, L. Kong, et al., Small 20 (2024) e2309599.
[24] M. Gunnarsson, E.H. Mojumdar, D. Topgaard, et al., J. Colloid Interface Sci. 604 (2021) 480–491.
[25] E. Sparr, S. Björklund, Q.D. Pham, et al., Curr. Opin. Colloid Interface Sci. 67 (2023) 101725.
[26] Y.C. Huang, Q.P. Cheng, U.S. Jeng, et al., ACS Appl. Mater. Interfaces 15 (2023) 5798–5810.
[27] W. Choi, J. Hong, Acta Biomater. 195 (2025) 216–224.
[28] H. Dai, X. Li, J. Du, et al., Food Hydrocoll 101 (2020) 105557.
[29] H. Cui, J. Cai, H. He, et al., Int. J. Biol. Macromol. 255 (2024) 127952.
[30] S.C. Millik, N. Sadaba, S.L. Hilburg, et al., Biomacromolecules 26 (2025) 1725–1736.
[31] M. Luo, Y. Wang, C. Xie, et al., Adv. Healthc. Mater. 11 (2022) e2200722.
[32] X. Zhao, J. Luo, Y. Huang, et al., ACS Nano 17 (2023) 22015–22034.
[33] S. Shang, K. Zhuang, J. Chen, et al., Bioact. Mater. 34 (2024) 298–310.
[34] H. Xie, Z. Wang, R. Wang, et al., Adv. Funct. Mater. 34 (2024) 2401209.
[35] R. Shaw, K. Patel, N.M.A. Chimthanawala, et al., Adv. Healthc. Mater. 14 (2025) e2403560.
[36] Y. Cao, N. Li, M. Chen, et al., Chem. Eng. J. 508 (2025) 160984.
[37] P. Li, Y.F. Poon, W. Li, et al., Nat. Mater. 10 (2011) 149–156.
[38] Y. Liu, H. Zhang, M. He, et al., Int. J. Biol. Macromol. 298 (2025) 139525.
[39] J. Liang, J. Ling, D. Sun, et al., Adv. Healthc. Mater. 13 (2024) 2400494.
[40] L. Ren, Z. Zhang, S. Yang, et al., Int. J. Biol. Macromol. 320 (2025) 145697.
[41] X. Xie, H. Lei, D. Fan, J. Mater. Sci. Technol. 144 (2023) 198–212.